Spatial confinement modulates macrophage response in microporous scaffolds

Yining Liu (yining.liu@duke.edu)[1]*
Alejandra Suarez-Arnedo (alejandra.suarez.arnedo@duke.edu)[1]*
Lindsay Riley (lindsay.riley@duke.edu)[1]
Tasman Miley (tasman.miley@duke.edu)[1]
Tatiana Segura (tatiana.segura@duke.edu)[1,2†]

[1]Department of Biomedical Engineering, Duke University
[2]Clinical Science Departments of Neurology and Dermatology, Duke University

* These authors contributed equally to the study
† To whom correspondence should be addressed to
Tatiana Segura
tatiana.segura@duke.edu

Abstract

Macrophages are essential in the initiation, maintenance, and transition of inflammatory processes like foreign body response and wound healing. These sentinel cells are very motile, susceptible, and adaptive to environmental cues. Mounting evidence suggests that physical factors also modulate macrophage activation *in vitro* and *in vivo*. 2D *in vitro* systems have demonstrated that constraining macrophages to small areas or channels modulates their phenotypes and changes their responses to known inflammatory agents such as lipopolysaccharide. However, macrophage responses in these 2D systems cannot be directly correlated to an *in vivo* response. Thus, the study of macrophage confinement in a 3D environment that can be directly used *in vivo* is needed and would allow the design of more translatable biomaterials for clinical applications. In this work, we explored the change in M1/M2 polarization when macrophages were confined in microporous annealed particle scaffolds (MAPS), which are granular hydrogels generated from annealed spherical microgels. We cultured primary murine macrophages within MAPS constructed of microgels with diameters of 40 µm, 70 µm, and 130 µm. Spatially confining macrophages in scaffolds with pore size on the scale of cells led to a reduced level of the inflammatory response, which was correlated with a change in cell morphology and motility.

Introduction

Macrophages are central to many injuries and diseases[1]. During a typical episode of inflammation, macrophages are among the first responders to arrive and polarize into a variety of activation states to perform specific functions. These states can be simplified as a spectrum from pro-inflammatory (M1) to pro-reparative (M2) phenotypes[2,3]. Generally, M1 phenotypes are associated with the initiation and maintenance of inflammation while M2 phenotypes are closely tied to the resolution of inflammation and the changeover to the regeneration phase[4]. Besides the intrinsic differentiation pathways governing this timely transition in phenotypes, macrophages are also adaptive to microenvironmental cues from the extracellular matrix they reside in and the neighboring cells[5]. Biochemical factors secreted by other cells, like IFN-γ or IL-4, can direct macrophages into pro-inflammatory or pro-reparative phenotypes[6]. The molecular mechanisms behind these common soluble factors and their effects on macrophages have been extensively studied. However, how physical signals regulate macrophage activation is less explored[7-9]. In the field of biomaterials, researchers have tested the influences of a wide range of material properties on macrophage modulation in pursuit of better biocompatibility. For example, surface modification by changing the hydrophilicity or decorating with cell binding ligands can lead to a reduction in macrophage attachment or a bias in macrophage polarization, respectively[10-13]. Understanding the specific mechanotransduction mechanisms that govern phenotypic macrophage changes will guide future biomaterial design and achieve a far-reaching physiological significance.

Spatial confinement (SC) is a well-known parameter to regulate macrophage response in the context of tissues or material scaffolds. Using topography design to force macrophages into an elongated cell shape has been shown to promote a pro-regenerative M2 phenotype[14]. Preventing mouse bone marrow-derived macrophages or RAW264.7 cells from spreading by spatial confinement, through the form of micropatterned surface, microporous substrates, or cell crowding, suppresses late lipopolysaccharide (LPS)-related transcriptional programs and cytokine expression[15]. This was explained by the limited actin polymerization in macrophages within a confined space and the subsequently reduced nuclear translocation of the actin-dependent transcription co-factor, myocardin-related transcription factor-A. This factor regulates

the LPS-stimulated inflammatory response so its reduction would result in a lower phagocytic potential and less pro-inflammatory cytokine secretion. Macrophages undergoing spatial constraints also endured chromatin compaction and epigenetic alterations (e.g., reduced histone deacetylase 3 level and enhanced H3K36-dimethylation). These findings uncovered some key pathways that guide macrophage response to SC. A precisely defined fiber poly(ε-caprolactone) scaffold with 40 µm box-shaped pores was shown to facilitate the most cell elongation in primary human macrophages, driving a M2-like polarization with increased M2 gene expression (CD206, CD163, IL-10) and reduced M1 activity (inflammatory cytokine expression and phagocytic activity)[16]. Together, these studies support the notion that the modulation of macrophage cell shape by spatial confinement impacts macrophage response. Studying this topic in a more physiologically relevant cell culture platform with a range of independently controlled properties is needed to better recapitulate macrophages' structures and functions *in vivo*[17].

In the past decade, granular materials emerged as an option for well-defined *in vitro* systems with plug-and-play components and tissue-mimicking 3D environments[18]. Specifically, the feature of tunable porosity makes these materials an ideal platform to study how SC impacts macrophage response. Here, we used microporous annealed particle scaffolds (MAPS), a type of granular material with an interlinking microgel network, as our 3D culture system and explored macrophage response within MAPS made of small (40 µm), medium (70 µm), and large (130 µm) diameter microgels. We discovered that confining macrophages in 3D MAPS changed their responses to M1 and M2 stimuli, and the activation levels of macrophages were correlated with changes in morphology, cell motility and nucleus shape regulated by the scaffolds.

Results

<u>Macrophages showed divergent morphologies upon spatial confinement in MAPS</u>

Using microfluidic devices, we generated microgels of three distinct sizes (40 µm, 70 µm, and 130 µm diameter), where each microgel possessed identical chemical components and mechanical properties. These microgels then formed three corresponding MAPS, i.e., small, medium, and large (s-, m-, l-MAPS, respectively), with similar void fractions of 25-35% and distinctly different internal landscapes (Figure 1a-c). We analyzed microscopic fluorescent images of MAPS using analytical software developed in-house for granular material analysis (LOVAMAP)[19], which segments the void space into subunits that represent the natural open pockets of space where cells may reside. The volume of the majority of subunits in s-MAPS fell below the average volume of a bone marrow-derived macrophage (BMDM) and closely resembled the confined condition in a related macrophage spatial confinement study[15] (Figure 1d). m-MAPS had a median subunit volume similar to the average size of BMDM, whereas the subunits in l-MAPS were larger than BMDM and therefore imposed the least spatial confinement on the cells (Figure 1d). Internal doors are the interfaces between neighboring subunits through which cells move to traverse from one subunit to the next. The range of internal door diameters in s- and m-MAPS fell below the diameter of a BMDM, meaning that when cells passed through these doors they needed to deform (Figure 1e). When BMDM were encapsulated in MAPS at the same seeding density (10,000 cells per µl), a significantly higher number of cells were trapped and confined in s-MAPS compared to m-MAPS and l-MAPS, whose larger void space allowed cells to fall through before they adhered (Figure 1f,g). Without any additional stimulation, macrophages either remained in single cells or formed clusters of more than two cells (Figure 1f). The cell cluster to total cell number ratio was similar across different scaffold types,

indicating that BMDM forming cell clusters were independent of the number of subunits ("pores") dividing up the space or the level of spatial confinement within each subunit (Figure 1h). A divergent size-dependent morphology change was observed and characterized by the unit of a single cell or a cell cluster (Figure 1i-m). The cell area and volume of both single cell and cell cluster in l-MAPS showed a wider distribution given the larger subunit volume for cells to reside in (Figure 1i,j). The ellipticity value characterizes the elongation of the cell/cluster by fitting an ellipsoid inside and calculating the degree of deviation from circularity. The ellipticity prolate and oblate represents the directionality of the longer axis of the ellipsoid, with prolate ellipsoid lengthening vertically and oblate ellipsoid flattening horizontally. A significantly lower ellipticity (prolate) for both single cell and cell clusters was observed in l-MAPS (Figure 1k) but not for ellipticity (oblate) (Figure 1l), suggesting a more elongated cell shape in the vertical direction directed by both the subunit volume and gravity. The sphericity of the cell unit in s-MAPS and l-MAPS was drastically lower than in m-MAPS (Figure 1m), which again pointed to a less spherical, more rough-edged morphology in these two types of scaffolds. The size-dependent change in cell morphology was also mirrored in the nucleus shape change, where l-MAPS promoted a significantly larger nuclei area (Supplementary Figure 1a,b). Both s- and l-MAPS elicited a more elongated and less circular nuclei shape (Supplementary Figure 1c-e). Previous studies have also demonstrated that changes in cell shape led to nuclear morphology changes and thereby causing the reorganization of nuclear components[14]. The elevated cell elongation observed in s- and l-MAPS was associated with a more elongated nuclei shape, which was previously linked to a higher degree of chromatin condensation[20] and histone acetylation[21]. Since macrophage M1/M2 response is associated with distinct morphological changes in 2D, we next set out to explore whether the activation-related morphology change would also be observed in 3D culture and impacted by the pore size difference.

Large MAPS promoted macrophage elongation in cell clusters upon M2 activation

In 2D culture, M2 activation of BMDMs with IL-4/IL-13 was correlated with an elongated cell shape[14] while M1 LPS activation was identified with larger nuclear areas and cell areas as well as a circular cell shape (Supplementary Figure 2a-c)[15]. Forcing macrophages into an elongated cell shape with a topography design is known to promote a pro-regenerative M2 phenotype[14]. On the other hand, spatially confining macrophages and thereby restricting cell spreading reduced macrophage inflammatory response to LPS[15]. Upon M1(LPS/IFNγ) or M2(IL-4) activation, macrophages remained in single cells or formed clusters of more than two cells (Figure 2a,b). The cell count per scaffold and the cell cluster ratio were at a similar level with or without activation (Supplementary Figure 3a,c). M2 activation in 3D culture led to an increase in cell area and volume, and a decrease in sphericity, all of which corresponded to a more elongated cell shape (Figure 2c-e). Notably, upon M2 activation, the cell area and volume of cell clusters in l-MAPS, which were already slightly elevated without any stimulation, were drastically increased (Figure 2c,d). The sphericity of cell clusters and the ellipticity values (prolate) of both single cell and cell clusters in l-MAPS also decreased significantly (Figure 2e, Supplementary Figure 3e). Collectively, these results suggested that l-MAPS promoted macrophage spreading, an M1-associated cell shape, in cell clusters upon M2 activation. M2 activation reduced the sphericity in both single cell and cell cluster in m-MAPS when compared to the M0 group. These changes observed in m-MAPS and l-MAPS, but not in s-MAPS, supported that both physical cues (spatial confinement) and biochemical cues (cytokine activation) act synergistically to modulate macrophage cell shape. Based on the connection between macrophage phenotype and cell shape, we hypothesized that macrophage functional response to M1/M2 stimuli in MAPS would also vary based on the level of spatial confinement.

Size dependent macrophage M1/M2 responses in small, medium, and large MAPS

When activated with M1(LPS/IFNγ) or M2(IL-4), 2D cultured BMDM showed a distinct activation response: M1 stimulation promoted the expression of pro-inflammatory markers inducible nitric oxide synthase (iNOS) and CD86 as well as antigen-presenting marker MHCII; pro-regenerative markers CD206 and Arginase 1 (Arg1) as well as antigen-presenting marker CD11c were drastically increased upon M2 activation (Supplementary Figure 2d-f). Therefore, these six markers were selected to further characterize macrophage activation in MAPS. After overnight culture in MAPS without stimulation, BMDM showed a size-dependent phenotype profile. M1-related marker (iNOS, CD86, MHCII) expressions were all lower than the baselines (BMDM cultured on 2D non-tissue culture-treated plates) while the level of CD11c from M2-related markers was drastically improved compared with 2D (Supplementary Figure 4d-f). m-MAPS promoted a much higher level of CD206, CD11c, iNOS, and CD86 in comparison to l-MAPS and/or s-MAPS (Supplementary Figure 4d-f). Activating BMDM in MAPS with an M1 stimulus led to a significantly lower expression of both iNOS and CD86 compared to the 2D baseline (Figure 3a), which indicated a reduced BMDM inflammatory response in the 3D culture. m-MAPS promoted a much higher level of CD206 and CD11c and an upward trend in iNOS and CD86 levels in contrast to l-MAPS and/or s-MAPS (Figure 3a-c). All four markers followed the same trends as the M0 BMDM in m-MAPS (Supplementary Figure 4d,f). Remarkably, inflammatory cytokines TNF and IL-6 showed an SC-regulated response (Figure 3d). Both cytokine levels were reduced in 3D culture in accordance with the reduced pro-inflammatory marker expression (Figure 3a). s-MAPS drastically decreased TNF and IL-6 secretion compared to m-MAPS and l-MAPS (Figure 3d), similar to previously reported results that spatial confinement reduced TNF and IL-6 production in M1(LPS) activated BMDM[15]. Macrophages cultured in l-MAPS responded to M2 activation with a drastic reduction in M2-related marker expressions (Arg1, CD206, CD11c) and significantly highly pro-inflammatory marker levels (iNOS and CD86), which corresponded with the M1-associated cell shape this scaffold promoted upon M2 activation. Taken together, these results suggested that macrophage phenotype in s-, m-, l-MAPS followed a size-dependent response.

Macrophage phenotype landscapes were shaped by spatial confinement

In traditional flow cytometry characterization of macrophage phenotypes, like the one we used in Figure 3, the macrophage population was first gated as CD11b+F4/80+ live cells, then further characterized by their expression levels of each functional marker. Median Fluorescent Intensity (MFI) was output to compare the expression of markers across samples. This analysis was performed with the idea that macrophages, in this case, BMDM, are one uniform population with similar characteristics. However, macrophage functional heterogeneity is a well-established concept in the field. More and more studies have demonstrated that macrophages perform context-based functions and even within the same tissue, functionally and developmentally distinct macrophage populations can coexist[22]. In response to a combination of LPS/IFN-γ and IL-4/IL-13, BMDM exhibited a mixed activation state with CD206 and CD86 expression at the same time[23]. Therefore, viewing all BMDM cultured in one scaffold as a homogenous population would obscure important differences in macrophage response. FlowSOM is an unsupervised algorithm that can distinguish cell populations and reveal how multiple markers were behaving on all cells[24]. Using FlowSOM to analyze flow cytometry data allowed us to identify 8 macrophage subpopulations co-expressing multiple different markers (Figure 4a-c). These macrophage subpopulations were characterized according to the expression levels of each marker (shown in the table below panel c, “+” meant over 50% of the subpopulation expressed

that marker, color blocks corresponded to the expression level of each marker). The basal levels of Arg1 and CD206 expression in BMDM were due to the differentiation method we used, which is known to induce a less inflammatory, pro-regenerative phenotype[25]. 2D cultured BMDM were used in each treatment condition as a reference to identify the major cell types associated with the treatments. When BMDM were cultured on 2D non-tissue culture-treated plastic without any activation, the dominant cell types were populations 1, 2, and 3 (Figure 4a). Compared to the 2D group, BMDM cultured in MAPS showed a shift from population 1 to population 2, the latter exhibiting more MHCII and CD86. In MAPS groups, populations 2 and 3 also expressed a higher level of CD206, especially those cultured in m-MAPS (Figure 4d). Upon M1(LPS/IFNγ) activation, the major population in all groups was population 3, which expressed higher levels of CD11c, MHCII as well as iNOS and likely performed an antigen-presenting function (Figure 4b). Populations 1, 3, and 5 in MAPS groups drastically decreased iNOS expression, specifically in s-MAPS and m-MAPS, and thereby showed a reduced inflammatory response (Figure 4e). After M2(IL-4) activation, the main phenotypes in the 2D group were again populations 1, 2, and 3 (Figure 4c). The s-MAPS group had a significantly lower percentage taken up by population 3, the M1 activation-associated population, and drastically decreased CD206 expression in population 3 as well as lowering Arg1 expression in populations 2 and 3 (Figure 4f). Altogether, macrophage phenotype landscapes in MAPS were shaped by spatial confinement and the confined s-MAPS group showed distinctively lower responses towards M1 and M2 activation.

Spatial confinement influenced macrophage motility by changing cell trajectory and velocity

Macrophages serve as sentinel cells *in vivo* and are very motile, constantly surveying the peripheral of our body[3]. When BMDM were encapsulated in a 3D scaffold like MAPS, they actively explored the void space of MAPS by moving inside and across subunits as well as sensing the surface of the microgels (Figure 5a-c, Supplementary Video 1-3). Specifically, in s-MAPS, BMDM wrapped themselves around the small microgels, moving in a circle (Figure 5a, Supplementary Video 1). In m-MAPS, most BMDM settled into the pocket of subunits and moved from side to side on the surface of microgels (Figure 5b, Supplementary Video 2). Some BMDM in m-MAPS traveled from one subunit to the adjacent one through the internal doors (Supplementary Video 2). l-MAPS had the most erratic cell movement. BMDM in l-MAPS frequently traversed along the surface of the microgels and went through the internal doors into neighboring subunits (Figure 5c, Supplementary Video 3). By tracing cell displacement, we discovered that l-MAPS posed the least confinement over cell motility whereas BMDM movement in s- and m-MAPS was limited to the local subunits (Figure 5d-f). Both cell displacement and velocity were affected by M1/M2 activation, but M1 cytokines elicited the most distinct changes (Supplementary Video 4-9). l-MAPS had the least restriction over activation-related increase in cell motility, resulting in the largest maximum travel distance and median velocity (Figure 5g,h). Notably, microgel displacement also followed a size-dependent manner, with l-MAPS having the most microgel movement due to the rapid cell activity (Supplementary Video 3,6,9). This showcased the dynamic structure of the MAPS system that is responsive to the encapsulated cells. These results again suggested that spatial confinement, imposed by different MAPS, influenced macrophage motility by changing cell trajectory and velocity.

Conclusions

Macrophages adapt to the features and cues from the surrounding microenvironment. Emerging evidence supports the essential modulating role physical factors play in macrophage activation. Spatial confinement (SC), applied by the pore size and the internal landscape of biomaterials, was demonstrated to suppress macrophage LPS-related inflammatory responses in 2D

systems[15]. Gaining insights into how SC regulates macrophage activation in a 3D environment allows us to design more translatable biomaterials for clinical applications.

In this work, we explored the change in macrophage activity within confined and unconfined granular materials formed with small (40 µm), medium (70 µm), and large (130 µm) microgels, respectively. Spatially confining primary mouse macrophages in scaffolds with pore size on the scale of cells led to changes in M1/M2 response, which was associated with a change in cell morphology and motility. Specifically, l-MAPS with pore sizes that can accommodate ~40 µm diameter spheres promoted M1-associated cell shape change in cell clusters upon M2 activation. This was correlated with a drastic reduction in M2-related marker expressions (Arg1, CD206, CD11c) and significantly highly pro-inflammatory marker levels (iNOS and CD86) in M2 BMDM inside l-MAPS. On the other hand, spatially confining BMDM in MAPS drastically decreased TNF and IL-6 secretion, which showed a size-dependent trend. The size-dependent change in cell morphology matched with the nucleus shape change, where both s- and l-MAPS induced a more elongated and less circular nuclei shape. Cell motility, characterized by maximum travel distance and median velocity, was also regulated by subunit size and was least restricted in l-MAPS. These findings suggested that spatial confinement, imposed by the size of void space inside porous scaffolds, plays a key role in regulating macrophage response in 3D culture. Future directions diving deeper into the mechanotrasduction pathways governing this SC-regulated process in 3D culture can further empower biomaterial design to modulate macrophage response.

Author contributions

Both YL and ASA made substantial contributions to the design of the work, acquisition, analysis, and interpretation of data. LR provided conceptualization, data and analysis that contributed substantially to figure 1. TM performed part of the experiment and analyzed data that contributed substantially to figures 1 and 2. YL drafted the manuscript, and all the authors discussed the results and contributed to writing portions of the manuscript and editing the manuscript. TS provided guidance and discussion throughout the project, and made substantial contributions to experimental design, data analysis, and manuscript editing.

Acknowledgements

We would like to thank the National Institutes of Health (R01AI152568) and all the members of Segura and Collier lab at Duke University for the support. A special thank you to our lab alumnus Jingyi Xia for working on this project during her master program and contributing to the preliminary data for this work. Thank you to our lab alumni Jun Chen, Ph.D., Ethan Ho and our lab member Eleanor Caston for technical assistance in the early stages of this work. Thank you to Minerva Matos-Garner, MA from Duke Engineering Graduate Communications and Intercultural Programs for her constructive suggestions on the manuscript and her warm support during the writing process.

Conflict of interest disclosure

The authors declare no financial/commercial conflict of interest.

Data availability

The data that support the findings of this study are available from the corresponding authors upon reasonable request. Source data are provided with this paper.

Methods

Microgel generation and purification

Microfluidic devices and microgels were produced as previously described. Briefly, a precursor solution with 8-arm PEG Vinylsulfone, K-peptide (Ac-FKGGERCG-NH2, GenScript), Q-peptide (Ac-NQEQVSPLGGERCG-NH2, GenScript) and RGD (Ac-RGDSPGERCG-NH2, GenScript) in 0.3 M triethylamine (Sigma) buffer. The cross-linker solution was prepared by dissolving the di-thiol matrix metalloproteinase-sensitive peptide (GenScript) in distilled water at 12 mM and 10 µM Alexa-Fluor 647-maleimide. These solutions were filtered through a 0.22 um sterile filter before loading them into 1 ml syringes. The final microgels were made of 5% (w/v) 8-arm PEG Vinylsulfone with 500 uM K-peptide, Q-peptide, and RGD, respectively. For small and medium microgel generation, we used a four-inlet device with two inlets for the aqueous solutions (precursor solution and crosslinker solution) and the oil phases (heavy mineral oil with 1% v/v Span-80 as the pinching oil phase and heavy mineral oil with 5% v/v Span-80 and 3% v/v Triethylamine as the gelation oil phase). The microgel solution was collected and allowed to gel overnight at room temperature. For large microgel generation, we used a two-inlet device with one for the aqueous solution (pre-mixed the precursor solution with an equal volume of the crosslinker solution) and the oil phase (heavy mineral oil with 5% v/v Span-80). The microgels were collected in a Span-80 (5% v/v) and Triethylamine (3% v/v) oil bath and allowed to gel overnight at room temperature. These microgels were then purified by repeated washes with a HEPES buffer (0.3 M, pH 8.3 containing 1% Antibiotic-Antimycotic and 2% Pluronic) and centrifugation. The purified microgels were stored in a HEPES buffer (pH 8.3 containing 1% Antibiotic-Antimycotic and 10 mM $CaCl_2$) at 4°C. The size of the microgels was measured from microscopic pictures (Nikon C2 confocal microscope, Nikon Instruments Inc.) of three separate batches of microgels using a custom MATLAB code. For cell study, the microgels were swollen in the culture medium for 20 minutes before the study.

Generation of Scaffold from microgels and Mechanical Testing

Excess buffer from the fully swollen and equilibrated microgels were removed by centrifuging at 22 000 G for 5-20 minutes and discarding the supernatant. 1 µl thrombin (200 U/mL in 200 mM Tris-HCl, 150 mM NaCl, 20 mM CaCl2) and 2 µl Factor XIII (250 U/mL) were combined with 50 µl microgels and mixed via thorough pipetting and allowed to incubate at 37°C for 30 minutes to form a solid hydrogel. Storage moduli of the hydrogels were measured by a frequency sweep on rotational rheometry (Anton-Parr, MCR301) at a shear frequency range from 10^-1 rad/s to 10^2 rad/s with a strain amplitude of 1%.

Primary Murine Macrophages culture

Bone marrow-derived macrophages (BMDM) were isolated from 8-12 weeks old C57BL/6 (mix gender) in accordance with institutional and state guidelines and approved by the Duke University's Division of Laboratory Animal Resources (DLAR) under protocol A019-21-01. Animals were anesthetized, and the tibias and femurs were collected. The bone marrow was flushed out from the bones and broken into cell suspension by repeated pipetting. The cells were differentiated in a culture medium (10% heat-inactivated fetal bovine serum in Iscove's Modified Dulbecco's Medium, Gibco) with 15 ng/ml macrophage colony-stimulating factor (Peprotech). The medium was changed on day 1, day 4, and day 8. After full maturation, the

cultured cells were tested for murine macrophage pan marker CD11b and F4/80 by flow cytometry to confirm the macrophage percentage (CD11b+F4/80+).

Macrophage in vitro encapsulation in MAPS

BMDM were detached from the culture flask with TrypLE express enzyme solution (ThermoFisher). The cell pellet was prepared at a final concentration of 10,000 cells per µl of MAPS. Subsequently, 50 µl of microparticle mixture containing Factor X/Thrombin was added to the cell pellet and thoroughly mixed before pipetting onto a sigmacote-treated glass slide. The slide was then placed into a petri dish and incubated at 37 °C for 45 minutes before transferring to a 6-well plate with the cell culture medium. For imaging purposes, the mixture was injected into the center of a cell culture device made in-house with a coverslip bottom. BMDM were cultured overnight in MAPS before the 24-hour cytokine activation. M1 activation was with 20 ng/ml LPS (ThermoFisher) and IFN-γ (Peprotech) and M2 activation was with 20 ng/ml IL-4 (Peprotech).

Live cell imaging and analysis

10 µl MAPS with encapsulated BMDM (10,000 cells/µl) were casted in 35 mm dish with 20 mm glass in the bottom (MatTek) and immediately imaged on an Olympus VivaView FL Incubator microscope (20x air objective). After 45 minutes, 3 ml of cell culture medium was added to the dish. The samples were activated with M1/M2 cytokines after 17 hours and imaged for another 27 hours. Images were taken at an interval of 30 minutes. For analysis, at the 24-hour mark, 10 cells were chosen at random. These 10 cells were tracked using the manual tracking feature in Fiji software (ImageJ), which allows the user to mark the location of each cell in every frame. If a cell disappeared from view at any point, tracking was stopped to ensure all data points could be attributed to only one cell. The data collected for three videos per scaffold were used to create the plots of cell displacement and determined the median velocity and max distance traveled by the cells in each scaffold.

IHC staining

At the designated time points, the samples were fixed with 4% PFA overnight at 4°C or 15 minutes at room temperature and then blocked with 0.3% Triton X-100 in 1xPBS for 10 minutes at room temperature. This was followed by staining for F-actin via Alexa Fluor 488/rhodamine phalloidin (Life Technologies) overnight at 4 °C. The scaffolds were then washed with 1X PBS, followed by counterstaining with a DAPI solution in 1X PBS for 15 minutes at room temperature. The samples were imaged with a Nikon C2 confocal microscope (Nikon Instruments Inc.), using a 40x magnification water immersion lens. The height of image stacks was set at 130 µm and the total number of slices was 260.

Cell morphology analysis

To analyze cell morphologies within the scaffolds, cell renderings were created of the 3D confocal images (40x objective) using the IMARIS x64 software (Oxford Instruments). To complete these renderings, both “spots” and “surfaces” functions were used. First, a computer-generated plot was created in the DAPI channel to visualize the cell nuclei and 9 µm was chosen as an estimation of the nuclei size. By overlaying the original image on top of the generated spots, background signals and nuclei without any actin filament around them were removed from the plot. A similar process was used with the “surfaces” function to view the morphology of the cells. The renderings were completed with the surface detail set at 1 µm. The

absolute intensity threshold was adjusted manually to ensure that the surface matched the actin filaments in the actual images. A baseline of absolute intensity threshold was chosen for each scaffold type and minor adjustments were made to avoid over- or under-rendering. Cell clusters were defined as any surface containing two or more nuclei and were therefore analyzed as one unit. Cell surfaces without a nucleus in close proximity were removed manually. For all the surfaces created, a list of parameters was generated for further analysis: sphericity, ellipticity, volume and area of a single cell and a cell cluster, total cell count, cluster number, and single cell number.

Nuclei morphology analysis

To analyze nuclear shape within the scaffolds, mean Z-stack projection images were generated using Fiji software (ImageJ). After splitting and thresholding in the DAPI channel with “Intermodes" method, the binary image was processed with “fill holes” and “watershed” functions. Four parameters were calculated: nuclei area, circularity (defined as “4*pi(area/perimeter^2)”), roundness (defined as “4*area/pi*sqr(major axis)”), and aspect ratio (defined as “major axis/minor axis”).

Flow cytometry study

At the designated time points, the cells were extracted from MAPS by enzymatic digestion of the gel with the digestion solution (200 U/ml Collagenase IV and 125U/ml DNase I) in RPMI media for 10 minutes at 37 °C. The cells were washed once with 1xPBS and resuspended into a single cell suspension. These cells were then stained with a Zombie NIR (BioLegend) solution for 15 minutes at room temperature and blocked with Fcr Blocking Reagent (Miltenyi Biotec) for 10 minutes on ice, followed by surface marker staining for 30 minutes on ice. For intracellular marker staining, an intracellular fixation & permeabilization buffer set (Thermo Fisher) was used to prepare the samples. After staining, samples were washed and resuspended in 150 ul flow buffer (1x PBS, 1 mM EDTA, 0.2% BSA, 0.025% proclin) and analyzed on the Cytek NL-3000 Flow Cytometer. Data was acquired using SpectroFlo software and analyzed using FlowJo 8 (TreeStar) flow cytometry data analysis software. The relative abundance of the macrophage population was gated following the gating strategy. Relative abundance of macrophage subpopulations was determined as a fraction of CD11b+F4/80+ live cells (gated first on scatter FSCxSCC, then doublet discrimination via FSC-AxFSC-H, prior to Viability dye). Phenotype analysis was performed with the FlowSOM algorithm on a concatenated file with 5000 macrophages pooled from each sample and the main macrophage subpopulations were sorted into 8 metaclusters. Each subpopulation was further identified by the expression or absence of different phenotypical markers.

ELISA

Cell culture medium was collected from 2D and MAPS confined BMDMs after 24 h of cytokine stimulation. To remove cell debris, the cell culture medium was centrifuged, and the supernatant was collected and stored at -80 °C until further processing. All ELISA kits were purchased from ThermoFisher Scientific, and the tests were performed according to the manufacturer’s protocol.

Figures

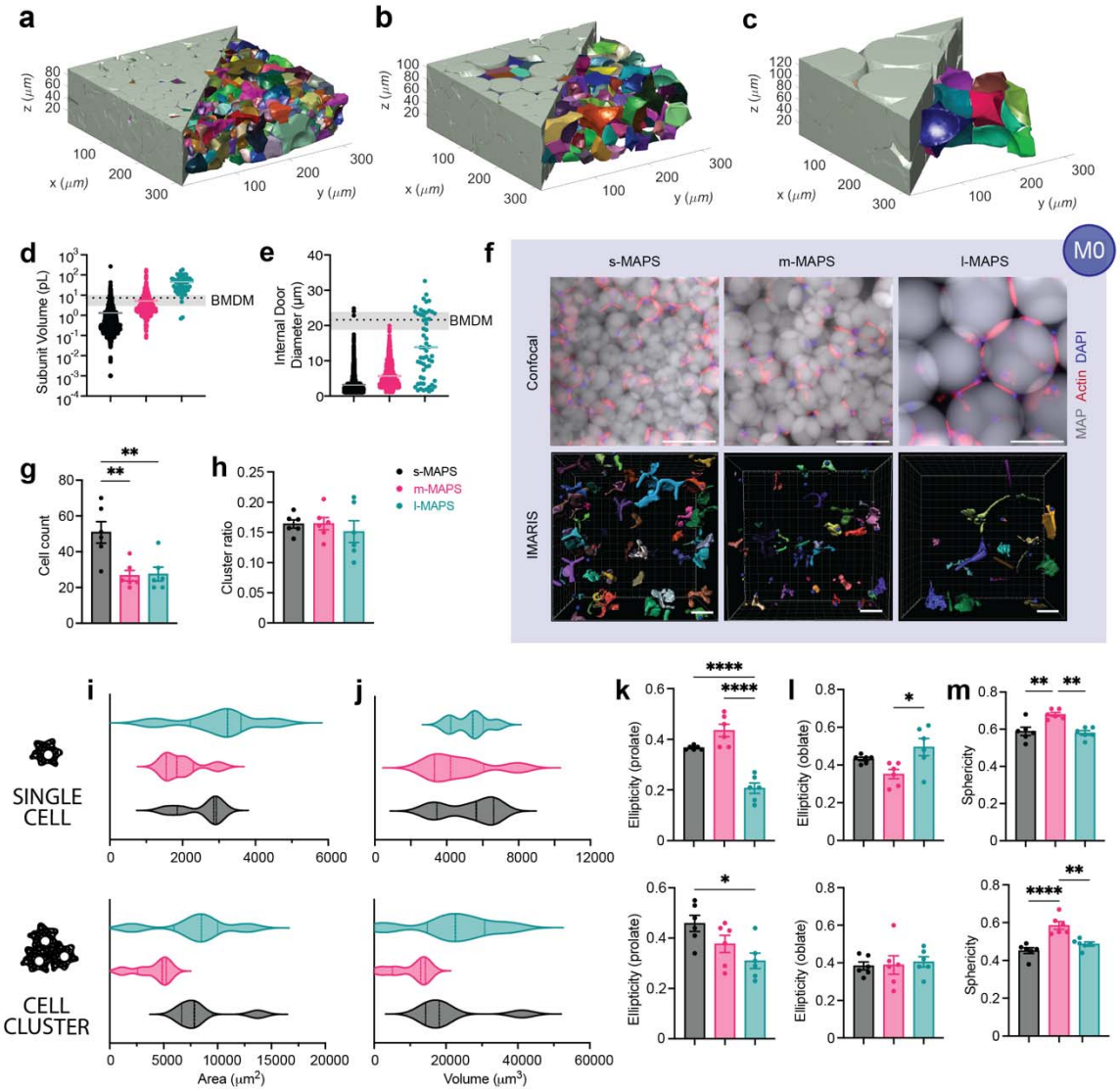

Figure 1 Macrophages showed divergent morphologies upon spatial confinement in MAPS. a-c, LOVAMAP analysis of microscopic fluorescent images of MAPS (grey spheres) with the colored void space subunits. d, the volume of the subunits for s-, m-, l-MAPS compared to the volume of bone marrow-derived macrophages (BMDM) in 3D culture. The black dotted line showed the average volume, and the grey area covered the standard deviation. e, the diameters of all the

internal doors for s-, m-, l-MAPS compared to the diameter of BMDM in 3D culture. The black dotted line showed the average diameter, and the grey area covered the standard deviation. f, fluorescent images showing BMDM encapsulated in MAPS without any activation (microgels in grey, actin filaments in red, the nucleus in blue, scale bar 100 μm) and the IMARIS software renderings of the single cells and cell clusters in MAPS (colored units, scale bar 50 μm). g, cell count in each type of scaffold. h, the ratio of cell cluster to the total cell count in each type of scaffold. i-m, morphology analysis for single cell (first row) and cell cluster (second row) of unstimulated BMDM in MAPS, showing cellular area distribution, volume distribution, ellipticity (prolate and oblate), and sphericity. Statistical analysis: one-way ANOVA with Tukey's multiple comparisons test made between s-, m-, l-MAPS groups only when there was significant difference among means. * $p<0.05$, ** $p<0.01$, *** $p<0.001$, **** $p<0.0001$. Error bars, mean ± s.e.m. n = 6 samples per scaffold type.

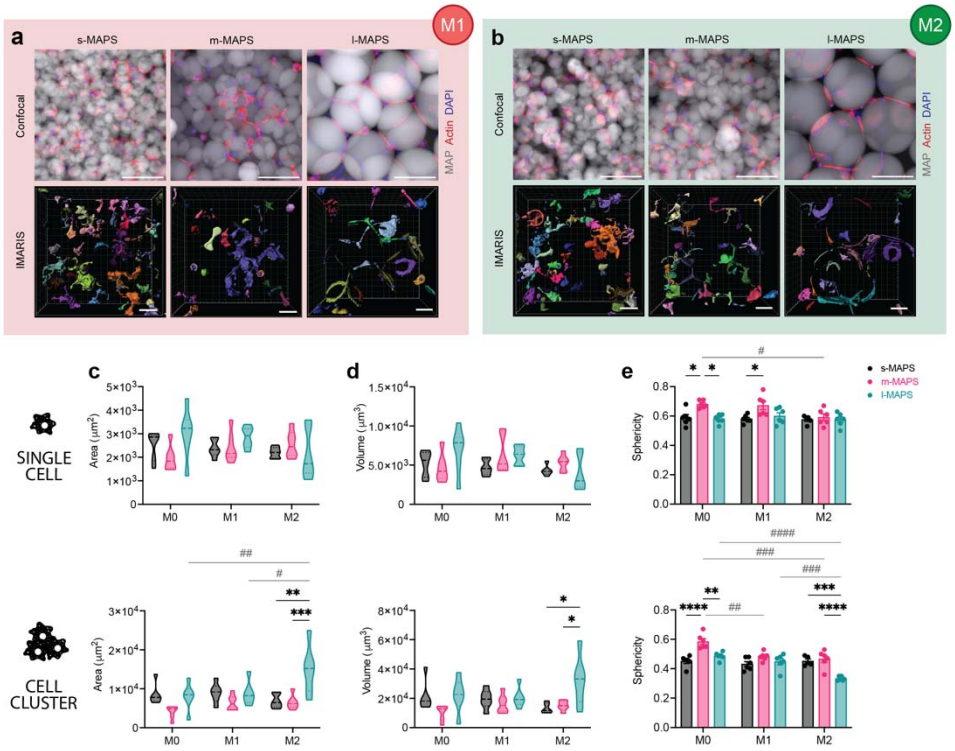

Figure 2 Macrophage morphologies in s-, m-, l-MAPS upon M1 or M2 stimulation were modulated by confinement. a, fluorescent images showing BMDM encapsulated in MAPS with M1(LPS/IFNγ) activation (microgels in grey, actin filaments in red, nucleus in blue, scale bar 100 μm) and the IMARIS software renderings of the single cells and cell clusters in MAPS (colored units, scale bar 50 μm). b, fluorescent images showing BMDM encapsulated in MAPS with M2(IL-4) activation (microgels in grey, actin filaments in red, nucleus in blue, scale bar 100 μm) and the IMARIS software renderings of the single cells and cell clusters in MAPS (colored units, scale bar 50 μm). c-e, morphology analysis for single cell (first row) and cell cluster (second row) of unstimulated/M0 or M1 or M2 BMDM in MAPS, showing cellular area distribution, volume distribution, and sphericity. Statistical analysis: two-way ANOVA with Tukey's multiple comparisons test made between s-, m-, l-MAPS groups only when there was a significant difference in scaffold type x treatment. * $p<0.05$, ** $p<0.01$, *** $p<0.001$, **** $p<0.0001$. Asterisks in black show difference within a treatment and between scaffold type. Pound signs in grey

show differences within a scaffold type and between treatments. Error bars, mean ± s.e.m. n = 6 samples per scaffold type.

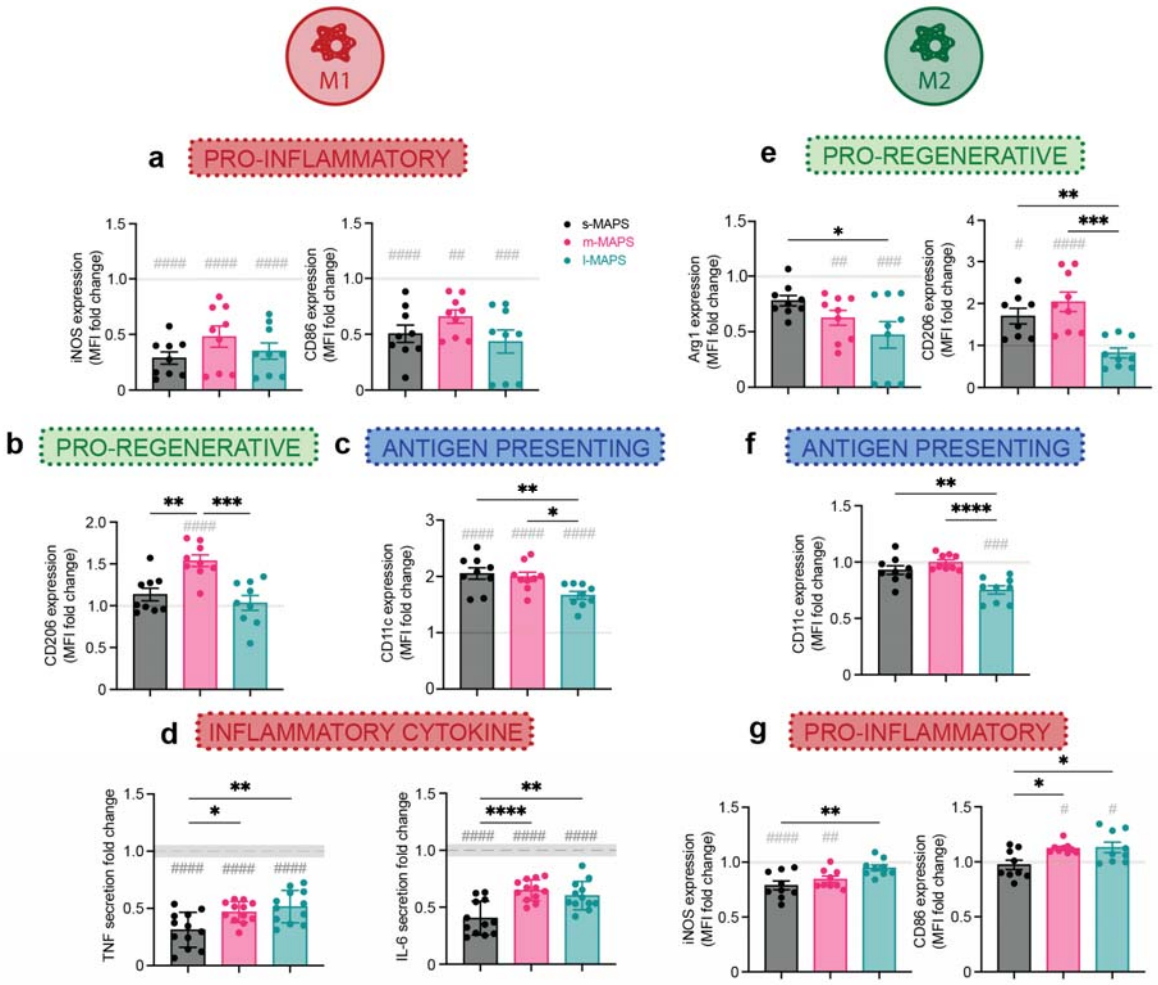

Figure 3 Macrophage M1/M2 responses in s-, m-, l-MAPS followed a size-dependent manner. a-c, the expression level (MFI fold change over the corresponding 2D culture with the same activation) of pro-inflammatory markers iNOS and CD86, pro-regenerative marker CD206, and antigen-presenting marker CD11c upon M1(LPS/IFNγ) activation. d, inflammatory cytokines TNF and IL-6 secretion fold change (over the corresponding 2D culture with the same activation) upon M1(LPS/IFNγ) activation. e-f, the expression level (MFI fold change over the corresponding 2D culture with the same activation) of pro-regenerative markers Arg1 and CD206, antigen-presenting marker CD11c and pro-inflammatory markers iNOS and CD86 upon M2(IL-4) activation. Statistical analysis: one-way ANOVA with Tukey's multiple comparisons test made between s-, m-, l-MAPS groups only when there was significant difference among means. Dunnet method was used in a separate one-way ANOVA to compare each treatment against 2D culture with the same activation as a baseline and the significances were indicated with gray ponds. */# $p<0.05$, **/## $p<0.01$, ***/### $p<0.001$, ****/#### $p<0.0001$. All the grey dotted baselines stand for the expression level in 2D culture with the same activation. Error bars, mean ± s.e.m. n = 9 samples from three independent experiments per scaffold type.

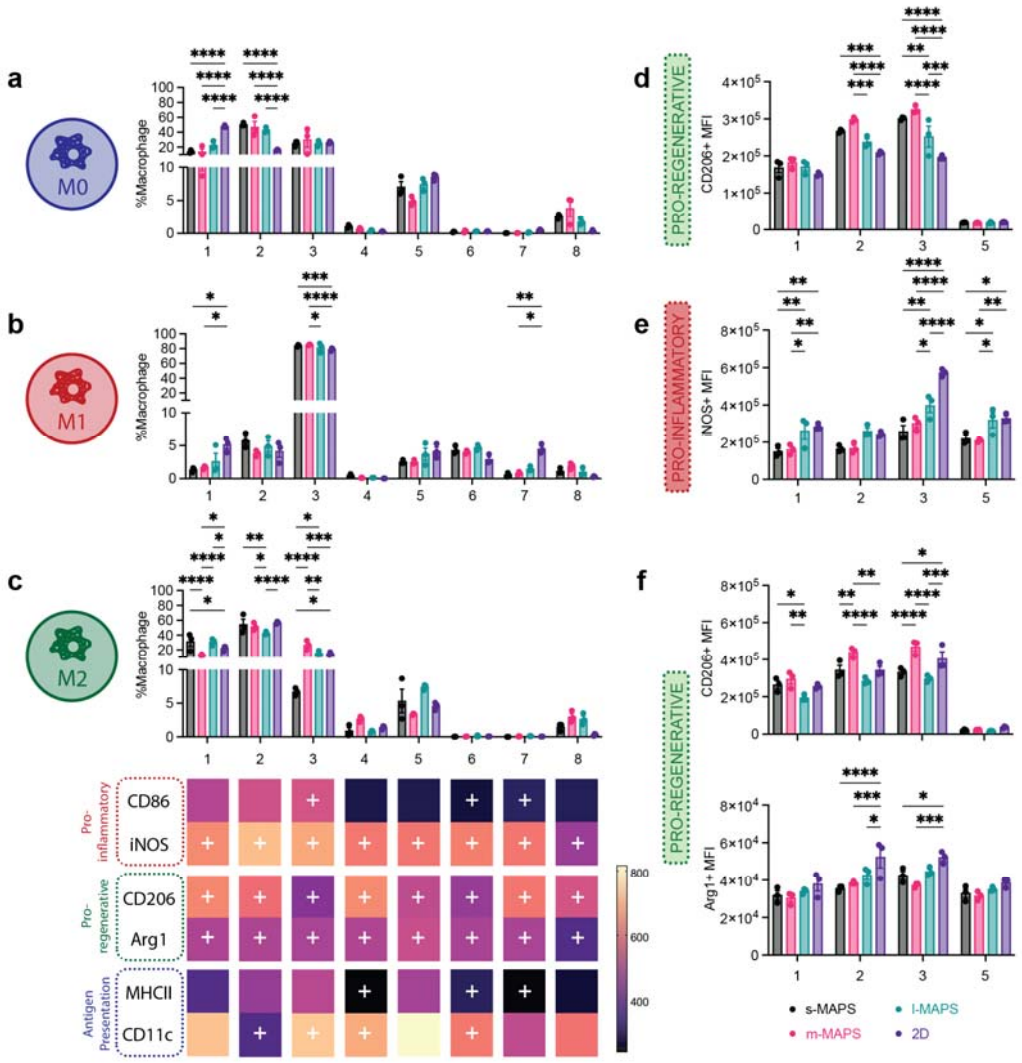

Figure 4 Macrophage phenotype landscapes were shaped by spatial confinement. a-c, the percentage of each macrophage subpopulation among the total macrophage population in s-, m-, l-MAPS or 2D groups without activation, upon M1(LPS/IFNγ) activation or M2(IL-4) activation. The table beneath it showed the expression levels of each marker in 8 different macrophage populations. "+" indicated that more than 50% of the population expressed that marker. The color blocks were corresponding to the MFI of each marker in each subpopulation. d, the expression level of pro-regenerative marker CD206 in macrophage subpopulations 1, 2, 3 and 5 without activation. e, the expression level of pro-inflammatory markers iNOS in macrophage subpopulations 1, 2, 3 and 5 with M1 activation. f, the expression level of pro-regenerative marker CD206 and Arg1 in macrophage subpopulations 1, 2, 3 and 5 with M2 activation. Statistical analysis: two-way ANOVA with Šídák's multiple comparisons test made between s-, m-, l-MAPS and 2D groups only when there was a significance in the interaction term of scaffold type x subpopulation. * $p<0.05$, ** $p<0.01$, *** $p<0.001$, **** $p<0.0001$. Error bars, mean ± s.e.m. n = 3 samples per scaffold type. The analysis was repeated for three independent experiments and only one set of results was shown here.

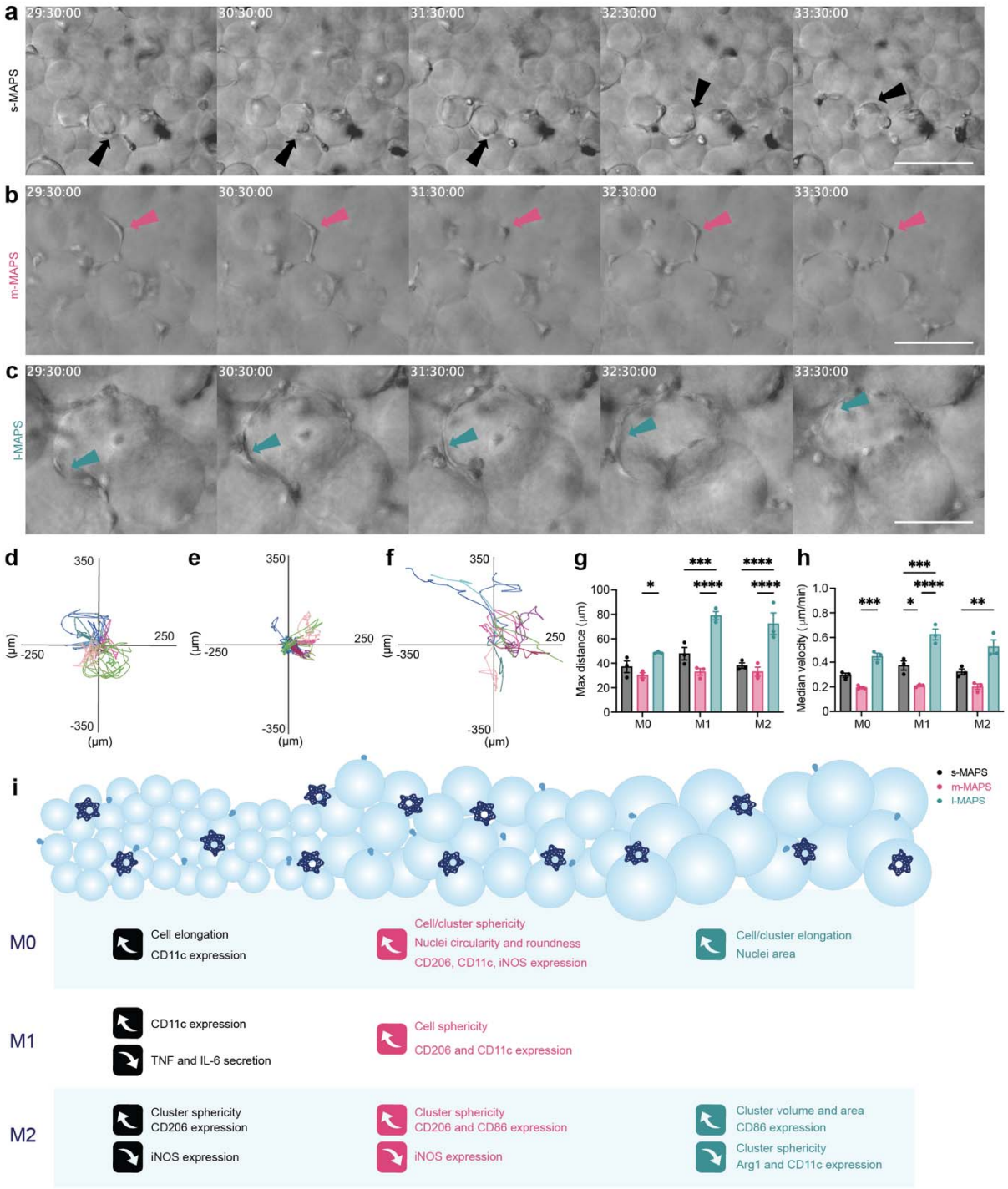

Figure 5 Spatial confinement influenced macrophage motility by changing cell trajectory and velocity. a-c, representative frames from live cell imaging video of BMDM in s-, m-, l-MAPS without activation. The arrows pointed to one representative cell in each scaffold. d-f, representative plots of BMDM displacement from origin for 20 hours in s-, m-, and l-MAPS. n=10 cells in each plot. g, maximum total travel distance of unstimulated/M0 or M1 or M2 BMDM in MAPS. h, median velocity of unstimulated/M0 or M1 or M2 BMDM in MAPS. i, schematic

summary of the main findings of this paper. Statistical analysis: two-way ANOVA with Tukey's multiple comparisons test made between s-, m-, l-MAPS groups only when there was a significant difference in scaffold type x treatment. * $p<0.05$, ** $p<0.01$, *** $p<0.001$, **** $p<0.0001$. Asterisks in black show difference within a treatment and between scaffold type. Error bars, mean ± s.e.m. n = 3 samples per scaffold type.

References

1 Gordon, S. The macrophage. *Bioessays* **17**, 977-986 (1995). https://doi.org:10.1002/bies.950171111

2 Wynn, T. A. & Barron, L. Macrophages: master regulators of inflammation and fibrosis. *Seminars in liver disease* **30**, 245-257 (2010). https://doi.org:10.1055/s-0030-1255354

3 Wynn, T. A., Chawla, A. & Pollard, J. W. Macrophage biology in development, homeostasis and disease. *Nature* **496**, 445-455 (2013). https://doi.org:10.1038/nature12034

4 Delavary, B. M., van der Veer, W. M., van Egmond, M., Niessen, F. B. & Beelen, R. H. J. Macrophages in skin injury and repair. *Immunobiology* **216**, 753-762 (2011). https://doi.org:https://doi.org/10.1016/j.imbio.2011.01.001

5 Mosser, D. M. & Edwards, J. P. Exploring the full spectrum of macrophage activation. *Nat Rev Immunol* **8**, 958-969 (2008). https://doi.org:10.1038/nri2448

6 Murray, P. J. *et al.* Macrophage activation and polarization: nomenclature and experimental guidelines. *Immunity* **41**, 14-20 (2014). https://doi.org:10.1016/j.immuni.2014.06.008

7 Liu, Y. & Segura, T. Biomaterials-Mediated Regulation of Macrophage Cell Fate. *Frontiers in Bioengineering and Biotechnology* **8** (2020). https://doi.org:10.3389/fbioe.2020.609297

8 McWhorter, F. Y., Davis, C. T. & Liu, W. F. Physical and mechanical regulation of macrophage phenotype and function. *Cell Mol Life Sci* **72**, 1303-1316 (2015). https://doi.org:10.1007/s00018-014-1796-8

9 Jain, N., Moeller, J. & Vogel, V. Mechanobiology of Macrophages: How Physical Factors Coregulate Macrophage Plasticity and Phagocytosis. *Annu Rev Biomed Eng* **21**, 267-297 (2019). https://doi.org:10.1146/annurev-bioeng-062117-121224

10 Brodbeck, W. G. *et al.* Biomaterial surface chemistry dictates adherent monocyte/macrophage cytokine expression in vitro. *Cytokine* **18**, 311-319 (2002). https://doi.org:10.1006/cyto.2002.1048

11 Antonov, A. S. *et al.* alphaVbeta3 integrin regulates macrophage inflammatory responses via PI3 kinase/Akt-dependent NF-kappaB activation. *J Cell Physiol* **226**, 469-476 (2011). https://doi.org:10.1002/jcp.22356

12 Blakney, A. K., Swartzlander, M. D. & Bryant, S. J. The effects of substrate stiffness on the in vitro activation of macrophages and in vivo host response to poly(ethylene glycol)-based hydrogels. *J Biomed Mater Res A* **100**, 1375-1386 (2012). https://doi.org:10.1002/jbm.a.34104

13 Cha, B. H. *et al.* Integrin-Mediated Interactions Control Macrophage Polarization in 3D Hydrogels. *Adv Healthc Mater* **6**, 1700289 (2017). https://doi.org:10.1002/adhm.201700289

14 McWhorter, F. Y., Wang, T., Nguyen, P., Chung, T. & Liu, W. F. Modulation of macrophage phenotype by cell shape. *Proc Natl Acad Sci U S A* **110**, 17253-17258 (2013). https://doi.org:10.1073/pnas.1308887110

15 Jain, N. & Vogel, V. Spatial confinement downsizes the inflammatory response of macrophages. *Nat Mater* **17**, 1134-1144 (2018). https://doi.org:10.1038/s41563-018-0190-6

16 Tylek, T. *et al.* Precisely defined fiber scaffolds with 40 mum porosity induce elongation driven M2-like polarization of human macrophages. *Biofabrication* **12**, 025007 (2020). https://doi.org:10.1088/1758-5090/ab5f4e

17 Van Goethem, E. *et al.* Macrophage podosomes go 3D. *Eur J Cell Biol* **90**, 224-236 (2011). https://doi.org:10.1016/j.ejcb.2010.07.011

18 Riley, L., Schirmer, L. & Segura, T. Granular hydrogels: emergent properties of jammed hydrogel microparticles and their applications in tissue repair and regeneration. *Curr Opin Biotechnol* **60**, 1-8 (2019). https://doi.org:10.1016/j.copbio.2018.11.001
19 Riley, L., Peter Segura, Tatiana. Void space and scaffold analysis of packed particles: applications in granular biomaterials. *Manuscript is under review.* (2022).
20 Versaevel, M., Grevesse, T. & Gabriele, S. Spatial coordination between cell and nuclear shape within micropatterned endothelial cells. *Nature communications* **3**, 1-11 (2012).
21 Li, Y. *et al.* Biophysical regulation of histone acetylation in mesenchymal stem cells. *Biophysical journal* **100**, 1902-1909 (2011).
22 Ghosn, E. E. *et al.* Two physically, functionally, and developmentally distinct peritoneal macrophage subsets. *Proc Natl Acad Sci U S A* **107**, 2568-2573 (2010). https://doi.org:10.1073/pnas.0915000107
23 Smith, T. D., Tse, M. J., Read, E. L. & Liu, W. F. Regulation of macrophage polarization and plasticity by complex activation signals. *Integrative biology* **8**, 946-955 (2016).
24 Quintelier, K. *et al.* Analyzing high-dimensional cytometry data using FlowSOM. *Nature Protocols* **16**, 3775-3801 (2021). https://doi.org:10.1038/s41596-021-00550-0
25 Fleetwood, A. J., Lawrence, T., Hamilton, J. A. & Cook, A. D. Granulocyte-macrophage colony-stimulating factor (CSF) and macrophage CSF-dependent macrophage phenotypes display differences in cytokine profiles and transcription factor activities: implications for CSF blockade in inflammation. *The Journal of immunology* **178**, 5245-5252 (2007).